

## LA-UR-13-27632

Approved for public release; distribution is unlimited.

Title: Enhanced Electron-Photon Transport in MCNP6

Author(s): Hughes, H. Grady III

Intended for: SNA & MC 2013 Joint International Conference on Supercomputing in Nuclear Applications + Monte Carlo, 2013-10-27/2013-10-31 (Paris, France)

Issued: 2013-10-01



**Disclaimer:**

Los Alamos National Laboratory, an affirmative action/equal opportunity employer, is operated by the Los Alamos National Security, LLC for the National Nuclear Security Administration of the U.S. Department of Energy under contract DE-AC52-06NA25396. By approving this article, the publisher recognizes that the U.S. Government retains nonexclusive, royalty-free license to publish or reproduce the published form of this contribution, or to allow others to do so, for U.S. Government purposes. Los Alamos National Laboratory requests that the publisher identify this article as work performed under the auspices of the U.S. Department of Energy. Los Alamos National Laboratory strongly supports academic freedom and a researcher's right to publish; as an institution, however, the Laboratory does not endorse the viewpoint of a publication or guarantee its technical correctness.

# Enhanced Electron-Photon Transport in MCNP6

H. Grady Hughes<sup>1\*</sup>

<sup>1</sup>Los Alamos National Laboratory, Los Alamos NM 87545 USA

\*Corresponding Author, E-mail: hgh@lanl.gov

Recently a variety of improved and enhanced methods for low-energy photon/electron transport have been developed for the Monte Carlo particle transport code MCNP6. Aspects of this development include a significant reworking of the MCNP coding to allow for consideration of much more detail in atomic relaxation processes, new algorithms for reading and processing the Evaluated-Nuclear-Data-File photon, electron, and relaxation data capable of supporting such detailed models, and extension of the electron/photon transport energy range below the traditional 1-kilovolt limit in MCNP, with the goal of performing transport of electrons and photons down to energies in the few-electron-volt range. In this paper we provide an overview of these developments.

**KEYWORDS:** *photon/electron transport; Monte Carlo; MCNP; single-event electron transport*

## I. Introduction

The Los Alamos Monte Carlo transport code MCNP6, now in its first production release,<sup>(1)</sup> is a major step forward for the MCNP family of codes. MCNP6 is the culmination of several years of work to combine all of the capabilities of MCNP5<sup>(2)</sup> and MCNPX,<sup>(3)</sup> to improve the resulting code system, and to include a number of new features as well. One of these new features is an extensive reworking of the coupled electron/photon transport capability. This work is based on the introduction of most of the electron, photon, and atomic relaxation data from the eighth release of the sixth version of the Evaluated Nuclear Data File<sup>(4)</sup> (ENDF/B VI.8) into MCNP6, and the development of transport methods to make use of these new data. In this paper we give an overview of this work, separating the discussion into the topics of photon enhancements, improvements in atomic relaxation, and a new single-event electron method.

## II. Photon Enhancements

The new data and methods for MCNP6 include extensions of photon cross sections to lower energies than previously available, addition of entirely new data specific to atomic subshells, and completion of the form factor data for coherent and incoherent scattering. In this section we briefly discuss these developments.

### 1. Extensions to Low Energies

The ENDF/B VI.8 database includes, for the 100 elements from  $Z = 1$  to  $Z = 100$ , tabulations of total cross sections as functions of photon energy for the four fundamental photo-atomic transport processes that have traditionally been considered in MCNP: coherent and incoherent scattering, photoelectric absorption, and electron/positron pair production. For the last of these, pair production, the data are essentially unchanged from previous MCNP libraries. (A

technical detail is that the ENDF data distinguish between pair and triplet production, but the ACE-format libraries used by the code combine both processes into simple pair production.) The other three processes also remain unchanged for the energy range above 1 keV. The important difference is that data for these three processes are now available to the code in the low-energy range from 1 keV down to 1 eV. This is a significant extension of the energy range over which useful calculations can be done. For example, for transport in oxygen using the new data one can see the effects on the total photon cross section of the four populated atomic subshells (K, L1, L2, and L3). With earlier data, the entire subshell structure was below the mandatory lower limit of 1 keV. As another illustration, Fig. 1 shows the total and four individual photoatomic cross sections for iron from the ENDF/B VI.8 library, clearly indicating the increased amount of information in the extended evaluation.

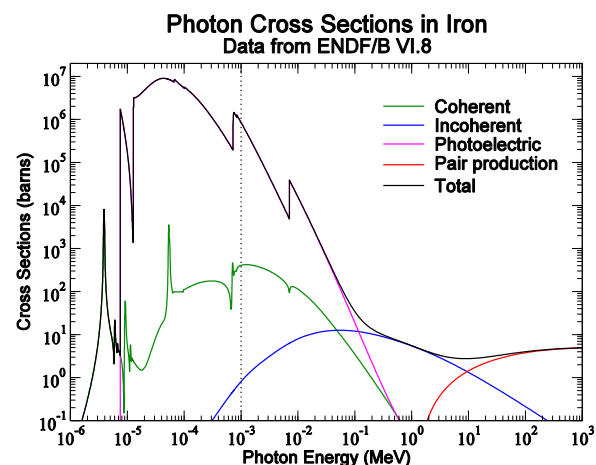


Figure 1. Photoatomic cross sections for iron, showing the energy range available with earlier data (above 1 keV) and the extended range from the ENDF/B VI.8 release.

## 2. Subshell-Specific Photoelectric Data

In addition to extending some pre-existing data to lower energies, the ENDF/B VI.8 database also includes several kinds of data that have not previously appeared in MCNP. The first such enhancement is the presence of subshell photoelectric cross sections. Previously only a total photoelectric cross section (as a function of energy) was given for each element, to be used in the selection of a distance to collision and a sampling of the collision process. With the improved data, the sampling of a photoelectric event can be followed by the detailed and accurate sampling of an individual subshell. The choice of vacated subshell determines the photoelectron energy and also determines the atomic relaxation cascade. Thus the treatments of photoelectric absorption, photoelectron generation, and subsequent relaxation are now managed more accurately, consistently, and with improved detail. These benefits apply even above the previous lower energy limit of 1 keV. To illustrate the new subshell-specific data, Fig. 2 shows the photoelectric cross sections for iron for all tabulated subshells.

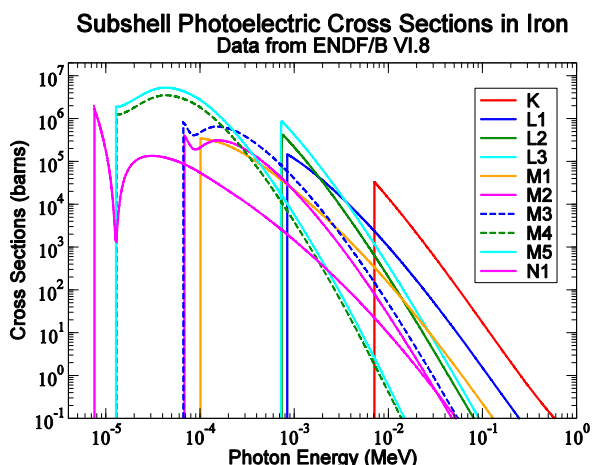


Figure 2. Subshell-specific photoelectric cross sections for iron for the ten tabulated subshell in the ENDF/B VI.8 release.

The direction of the photoelectron must also be found, and here we encounter one of only two aspects of the transport on which the ENDF/B VI.8 database is silent. Neither a data table nor an analytic prescription is available to address the issue. Therefore in MCNP6 we employ an algorithm<sup>(5)</sup> relying on precomputed tables based on work by Fischer and by Sauter.

## 3. Incoherent and Coherent Form Factors

For the angular distribution from incoherent photon scattering MCNP6 samples from a cross section

$$\sigma_{inc}(Z, \alpha, \mu) \propto I(Z, \nu)(\alpha'/\alpha)^2(\alpha'/\alpha + \alpha/\alpha' + \mu^2 - 1)$$

where the expression to the right of  $I(Z, \nu)$  is proportional to the Klein-Nishina cross section with  $\alpha = E/mc^2$ ,  $\mu = \cos \theta$ , and  $I(Z, \nu)$  is a tabulated form factor in terms of a convenient independent variable  $\nu = K\alpha\sqrt{1 - \mu}$  with  $K \approx 29.1445$  inverse ångströms. Similarly the coherent angular distribution is determined by a cross section

$\sigma_{coh}(Z, \alpha, \mu) \propto C^2(Z, \nu)(1 + \mu^2)$ , with a form factor  $C^2(Z, \nu)$  multiplied by the well-known Thomson cross section. In either case the photon scattering angle is determined by sampling from the product of two functions that can be treated as probability distributions.

In earlier versions of the code and cross section libraries, both form factor functions were tabulated only over a limited range ( $\nu \leq 8$  for incoherent scattering and  $\nu \leq 6$  for coherent). Consequently, representation of the scattering over the full angular range was complete only for a rather modest range of photon energies ( $E \lesssim 99$  keV for incoherent scattering, and  $E \lesssim 74$  keV for coherent scattering). The consequences of this incomplete representation are more severe for coherent scattering (where the missing data are treated as zero) than for incoherent scattering (where the missing data are forced to their asymptotic value of  $Z$ , the atomic number). Figure 3 illustrates the situation, showing incoherent and coherent cross section in lead for incident 150-keV photons. We see that for incoherent scattering, the old and new form factor data give reasonably similar results, with only a small artifact near  $\mu = 0.1$ , where the old data reach their limit and revert to a simple Klein-Nishina treatment for larger angles. By contrast the coherent cross section with form factors shows a radical difference between the new data and the old, where the cross section vanishes completely beyond a 60-degree scattering angle.

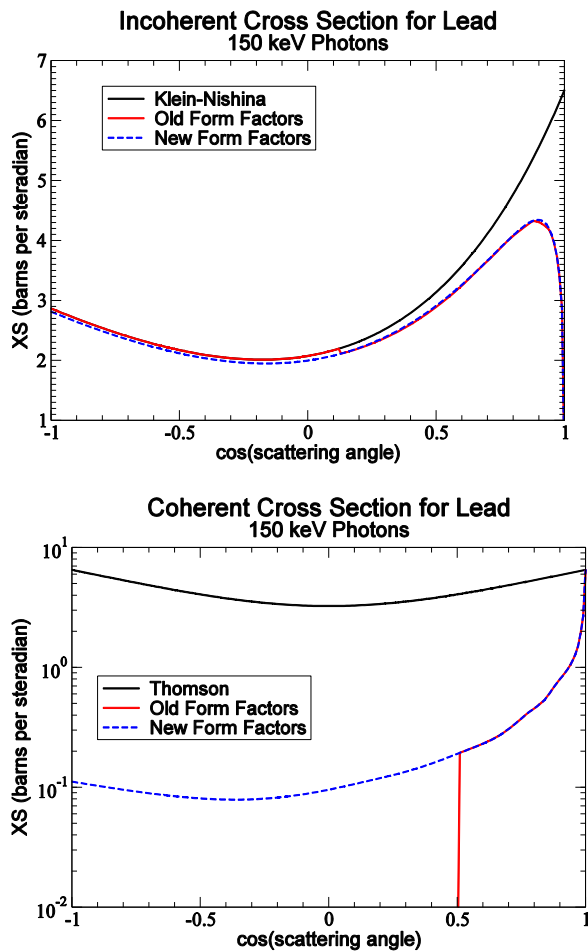


Figure 3. Incoherent and coherent cross sections for lead.

The ENDF/B VI.8 database extends both tabulations up to  $\nu = 10^9$ , a value large enough to guarantee full angular coverage over the entire energy range of the new data, up to 100 GeV. The particular modification to the ACE-format libraries supplying these data to MCNP6 follows earlier work<sup>(6)</sup> that was developed for several versions of MCNPX.<sup>(3)</sup> A further enhancement in the present work is the replacement of the previous linear interpolation of the form factors, no longer adequate for higher energies or larger scattering angles,<sup>(7)</sup> by a correct logarithmic method. This seemingly minor consideration can have a significant impact on the results of a calculation, as Figure 4 illustrates. Here we see an MCNP6 calculation of the coherent scattering angular distribution for 3-MeV photons on lead, showing the numerical artifacts that result from the no-longer appropriate linear interpolation contrasted with the more accurate new result.

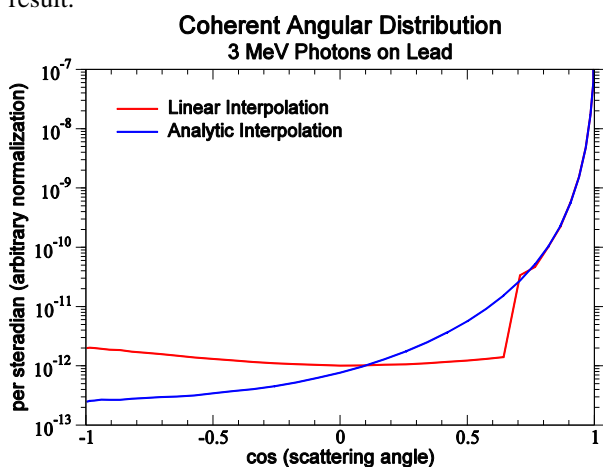


Figure 4. Coherent angular distribution for 3-MeV photons in lead, illustrating the old and new methods of form-factor interpolation.

### III. Enhancements in Atomic Relaxation

A very significant addition to the photon/electron data in MCNP6 is a detailed compilation of information about atomic electron subshells. The data now include the identities of all subshells that can play any non-negligible role in the atomic relaxation process for energies down to the new 1-eV lower limit, their binding energies, ground-state electron populations, and number of possible relaxation transitions. In contrast to the previous model, which considered only relaxations to the K shell and to a weighted average of the L shells and allowed a maximum of five distinct transitions to these shells, the new data can consider, depending on Z, as many as 29 subshells and can include almost 3,000 distinct transitions among them. For each possible transition to fill a vacancy in a given subshell  $S_0$ , the identity of the subshell  $S_1$  to receive the new vacancy (for a radiative transition) or the identities of the two subshells  $S_1$  and  $S_2$  to receive vacancies (for a non-radiative transition) are given, along with the line energy  $E_{012}$  of the fluorescent photon (or Auger or Coster-Kronig electron) and the probability  $P_{012}$  of this transition.

When a photoelectric event (or an electroionization event as

discussed in subsection 4.3 below) results in a vacancy in subshell  $S_0$ , the code can now survey the set of probabilities  $\{P_{0ij}\}$  for transitions that can fill the  $S_0$  vacancy, sampling a suitable instance ( $S_0, S_1, S_2$ ) with correct probability. An isotropically-directed photon (or electron) is then sampled, given the energy  $E_{012}$ , and banked for further transport. The vacancy in  $S_0$  is recorded as filled, and a vacancy appears in  $S_1$  (and in  $S_2$  for a non-radiative transition). Now, starting with  $S_1$ , the process is repeated until all subshells either are filled, or have no transitions provided in the database, or have all their transitions below the photon and electron energy cutoffs. This method, together with the enhanced database, provides a detailed simulation of the atomic relaxation cascade, and offers the possibility of complex spectroscopic simulations beyond the previous capabilities of MCNP. An illustration of this extended capability is given in Fig. 5, which contrasts the previous limited prediction with the newer result in the case of photon fluorescence from 100-keV photons interacting with an iron/tungsten target.

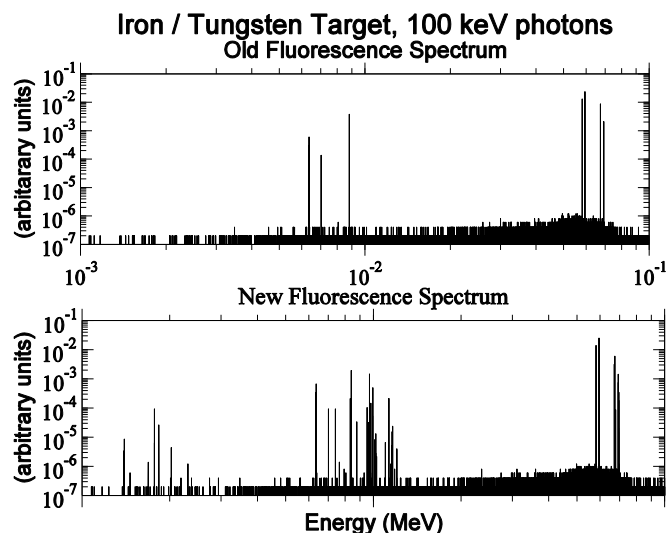


Figure 5. Predictions photon fluorescence using old and new atomic relaxation data.

### IV. Electron Enhancements

The ENDF/B VI.8 database provides microscopic cross sections and secondary distributions appropriate to the four fundamental electro-atomic transport processes: atomic excitation, electron elastic scattering, subshell electro-ionization, and bremsstrahlung. In all cases, tabulations of cross sections are given for energies between 10 eV and 100 GeV, and appropriate forms of tabulated distribution functions for secondary particles or energy loss are also provided. We will discuss some details of the data and sampling procedures for each process in turn. The reader will infer that these new procedures describe a completely different approach from the condensed-history method that previously was the only available algorithm for electron transport in MCNP. In this new single-event method we dispense with the multiple-scattering theories, substep-based approximations, uncorrelated processes, and other aspects of

the condensed-history approach, in favor of direct sampling of microscopic data distributions.

At the present stage of development, single-event electron transport is not intended to replace the condensed-history method in any energy range in which the traditional approach can be used. However, condensed-history electron transport in MCNP fails in the energy range below 1 keV because of specific limitations in the data and semi-analytic methods intended for higher energies. The single-event method now provides a successful and potentially more accurate approach to low-energy transport, and it is for this low-energy range that the new method was developed. Of course, the possibility of using single-event electron transport at higher energies is intriguing, but a large amount of validation and verification must be done before this application can be considered reliable. There are also significant performance issues, since the single-event method is inherently more computationally intensive than condensed history. These interesting questions are now beginning to be explored.

### 1. Atomic Excitation

Atomic excitation is the simplest of the four electron interactions both to describe and to implement. For each element two tables are provided: a tabulation of  $\sigma_{exc}(E)$ , the cross section for an excitation event, and  $\delta E_{exc}(E)$ , a tabulation of average energy loss due to excitation as a function of electron energy. In the code, for an electron of energy  $E$ , the cross section is found by interpolation in  $\sigma_{exc}(E)$ , a distance to collision is sampled and competes with distances to collision for the other processes. If excitation is selected, the energy loss is found by interpolation in  $\delta E_{exc}(E)$  and deducted from the current energy of the electron, which then continues transport. This process involves no angular deflection of the electron and no production of secondary particles.

### 2. Elastic Scattering

Electron elastic scattering is also a fairly simple process in that it involves no secondary particles and no energy loss by the electron. However the representation of the data for angular distributions and the sampling algorithms are somewhat more complex. The beginning of the process is similar to that of excitation. For an electron of energy  $E$ , the elastic cross section is found by interpolation in  $\sigma_{elas}(E)$ , which is tabulated from 10 eV to 100 GeV, and is used to sample a distance to collision, again competing with the other processes. When elastic scattering is selected, the code relies on a more elaborate collection of data. Rather than a single table for the results of the process, there are multiple tables (from 14 to 16 depending on the element) for selected electron energies. Each of these is a tabulation of angles, expressed as  $\mu = \cos \theta$ , and corresponding probability densities  $P(\mu)$  that can be converted into a form suitable for sampling. However the angular range for each table is not complete, but covers the angles from  $\mu = -1$  to a final angle  $\mu = \mu_N = 1 - 10^{-6}$ , about 1.4 milliradian from the forward direction. The intention of the evaluators is that the tabulated probabilities should be used for angles away from

the peak and an analytic function  $f(\mu) = A/(\eta + 1 - \mu)^2$  for angles near the peak, where  $\eta(E, Z)$  is proportional to a screening angle given by Seltzer<sup>(5)</sup> derived from the work of Molière,<sup>(8)</sup> and  $A$  is a normalization constant determined by the requirement that the table and function be continuous at  $\mu = \mu_N$ . This continuity condition is used to determine the probability that a given elastic event will scatter the electron into the peak or into the tabular angular region. Appropriate interpolation among the separate tabulations and the separate analytic forms then leads to the angular sample for a given elastic scatter.

This representation of the angular distribution has been and remains problematic. The tabulated data suffer from a limitation of the ENDF format, which is insufficiently precise to resolve satisfactorily the strong peak of the scattering distribution. Specifically, the  $\mu$ -values in the forward peak become increasingly imprecise (and in extreme cases, indistinguishable) just as the probability density becomes large. This circumstance results in some unsolved problems in the current model, both in the tabular and in the analytic domains. Fortunately this situation occurs primarily at high  $Z$ -values, and especially at high energies. Therefore there should be little effect of these issues for the low-energy applications for which the single-event model is currently intended. Nevertheless these matters are under active investigation.

### 3. Electroionization

Electroionization is mathematically simpler than elastic scattering, but features more levels of tabulation than that process. First there is a tabulated total ionization cross section  $\sigma_{ion}(E)$ , which is used to sample a distance to collision and to select among the four collision processes. Then for each atomic subshell provided in the atomic relaxation portion of the ENDF data, there is a tabulated cross section  $\sigma_{shell}(E)$ . When electroionization is selected, these partial cross sections are used to sample for the identity of the subshell that will be vacated by the ionization event. For each such candidate subshell, there are additional tables  $P_{knock}(E_\Delta)$ . As was the case for elastic scattering, there is one such tabulation for each of a number of energies spanning the range from 10 eV to 100 GeV. These tables, however, are representations of the probability distributions for the energy of the emitted secondary electron  $E_\Delta$  from ionization (the "knock-on" electron). When the electroionization process is selected and the particular subshell is chosen, the code then locates the electron energy  $E$  between adjacent energy points  $E_0$  and  $E_1$  for which there are  $P_{knock}(E_\Delta)$  tables. Correlated sampled values of the energy of the knock-on electron are obtained, and their linearly interpolated value  $E_\Delta$  is then determined. The energy of the incident electron is reduced by the value  $E_{bind} + E_\Delta$  which is the sum of the binding energy of the selected subshell and the kinetic energy given to the secondary electron. With knowledge of the energies, the polar deflections of both particles from the incident direction can now be calculated by conservation of momentum without further sampling. (In a minor departure from the otherwise analog nature of the single-event process, the

azimuthal angles are sampled independently, and do not lie in the same plane.) The knock-on electron is now banked for further transport, and the incident electron continues. In a distinct action, the identity of the vacated subshell may be sent to the new atomic relaxation routine to track the full relaxation cascade that results from this ionization event.

#### 4. Bremsstrahlung

The description of the bremsstrahlung process again begins with a tabulated cross section,  $\sigma_{brem}(E)$ , which is used to find a distance to collision and to select among the four collision processes. As in the elastic and electroionization cases, where a doubly-differential probability distribution must be represented, there is a collection of probability tables  $P_{brem}(E_\gamma)$  giving the energy spectrum of bremsstrahlung photons at several electron energies. When bremsstrahlung is selected, the code again finds the electron energy  $E$  between adjacent energy points  $E_0$  and  $E_1$  for which there are  $P_{brem}(E_\gamma)$  tables, obtains a correlated sample of the photon energy from each of the two tables, and determines  $E_\gamma$  as the linearly interpolated result for the bremsstrahlung photon energy. The energy of the incident electron is then reduced by  $E_\gamma$  and the electron continues transport.

It is assumed that the electron's direction is essentially unchanged by the bremsstrahlung event, but the direction of the photon must be determined. This is another issue for which the ENDF/B VI.8 database provides neither tabular probabilities nor an analytic prescription, leaving the matter up to the implementer of the transport code. For the single-event algorithm in MCNP6 we have developed an interim solution to this problem by using methods that were already in the code. If the electron's energy is above the range of the condensed-history data (above 1 GeV) then a simple analytic probability distribution

$$p(\mu)d\mu = \frac{1}{2} (1 - \beta^2) / (1 - \beta\mu)^2 d\mu$$

is used, where  $\beta = v/c$  and again  $\mu = \cos\theta$ . This is an appropriate distribution for high energies, and is also used in MCNP for bremsstrahlung contributions to point detectors and DXTRAN spheres.

If the electron's energy is within the range of the condensed-history model (1 keV to 1 GeV), then we invoke the table-based sampling scheme that has traditionally been used for sampling the bremsstrahlung photon angular distribution. This implies that the condensed-history data for an electron transport calculation must be initialized, even if the entire calculation is to be run with the new single-event model.

Finally, if the electron's energy is below the range of the condensed-history model (below 1 keV), then the analytic distribution  $p(\mu)d\mu$  is again used. This is not really

appropriate for low energies, and its presence in the current code is a temporary expedient. In a future version of the code this algorithm will be replaced by a more suitable model for low-energy radiation.

#### V. A Test Problem

Verification and validation of the enhanced electron, photon, and relaxation data and models are still in preliminary phases, but we are developing a useful collection of test problems and benchmark comparisons. Here we show results from one such test case. This problem considers the evolution of a monodirectional, monoenergetic 60-MeV electron beam transporting and diffusing in a large volume of dry air. This simple situation provides scope for a variety of investigations. For illustration here, we present only the spatial distribution of electron energy flux. We perform the calculation with three different options for the electron transport. First the standard condensed-history method is used with default values for the various transport controls. The result is shown in Fig. 6.

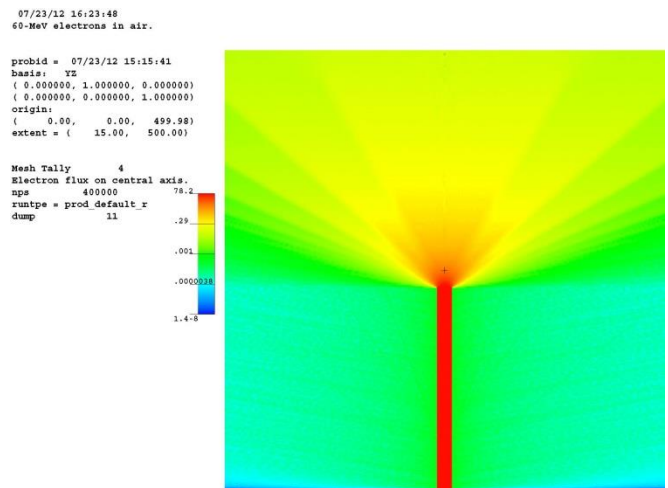
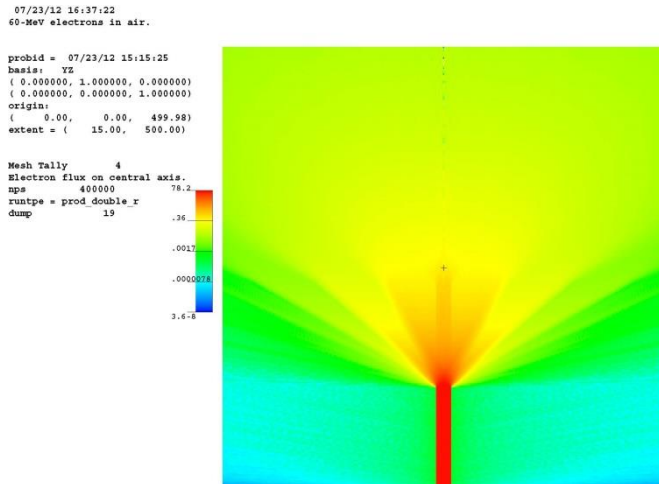


Figure 6. Electron energy flux from 60-MeV electrons in air. Standard condensed-history calculation.

We see quite clearly a well-known step-size artifact: the first angular substep occupies a significant part of the geometry of interest, and the condensed-history method in MCNP does not apply multiple-Coulomb energy loss or angular deflection until the end of the substep. We also see evidence of artifacts in the apparent ray effects in the angular distribution of the energy flux, a circumstance that has been less well studied.

It is well-known that the step-size artifacts in the condensed-history method can be ameliorated by increasing the number of angular substeps per energy step. When the calculation is performed with twice the default number of substeps, we see the result in Fig. 7.



**Figure 7. Electron energy flux from 60-MeV electrons in air. Condensed-history with increased number of substeps.**

Here we see an improvement in the spatial artifact (since the initial substep is only half of its original length), but the angular ray effects seem at least as prominent as before. Clearly this test problem will be a useful tool for exploring the transport physics of a variety of aspects of the condensed-history method. It is also interesting to try the new single-event method with this calculation. With that model, we find the results shown in Fig. 8.

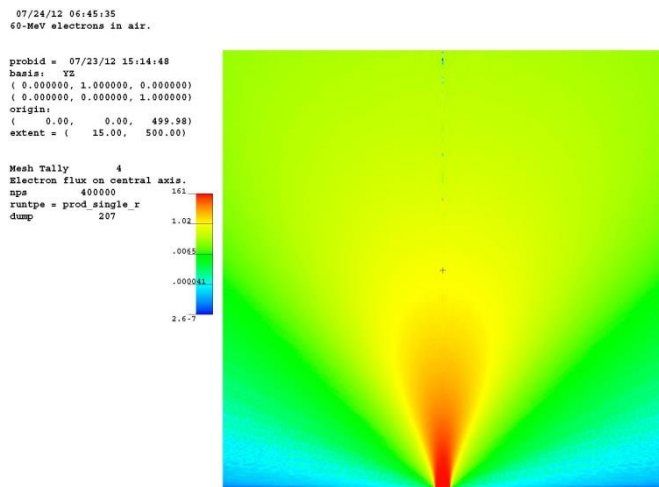


**Figure 8. Electron energy flux from 60-MeV electrons in air. Single-event electron transport.**

With the single-event method, both the spatial and the angular artifacts are gone. As discussed earlier, this initial development of the single-event method is only intended to support electron transport at energies below the traditional 1-keV lower energy limit of MCNP. This calculation, starting at 60 MeV and going down only to the usual 1-keV energy cutoff, is well beyond the energy range for which the method was created. Nevertheless, this encouraging result suggests that the single-event method may be a promising capability for a wider range of applications that might have been anticipated.

## VI. Limitations of the Method

The electron/photon transport models described here suffer from some limitations that should be mentioned. For example, the dramatically increasing uncertainty of the cross sections at extremely low energies is well-known.<sup>(9)</sup> Beyond this, all cross sections currently used for photons and electrons apply to cold, neutral, atomic target materials, and therefore omit any consideration of molecular effects, target thermal effects, material structure in condensed (solid or liquid) states, etc. Again these considerations matter most at extremely low energies. Also some theoretical advancements have not yet been brought into the methods, including photon polarization, anomalous scattering functions, synchrotron radiation, and ionization electrons from heavier charged particles (delta rays). A few advancements, including reflection and refraction for photons in or near the visible range and Cerenkov radiation, are not available in the current production release of MCNP6, but have been developed and will be included in a future release of the code.

## VII. Conclusion

With ENDF/B VI.8 data and new methods, MCNP6 has benefited from a significant advance in electron/photon transport capability. With these enhanced capabilities there is now a greatly expanded range of potential applications newly subject to Monte Carlo exploration with MCNP6.

## Acknowledgements

Many colleagues deserve thanks for help and collaboration, including Christopher Winstead, Christopher Walker, Grayson Rayborn, and the late Prof. Joon Lee of the University of Southern Mississippi; Robert Little, Jeremy Conlin, Morgan White, Kent Parsons, Michael James, Laurie Waters, Russell Johns, John Hendricks, Jeremy Sweezy, Jeff Bull, Richard Prael, Tim Goorley, Avneet Sood, Charles Lebeda, and John Zumbro of Los Alamos National Laboratory; D. E. Cullen of Lawrence Livermore National Laboratory; and Cecile Toccoli of CEA (France).

Initial development for this work was supported by the Defense Threat Reduction Agency. Ongoing MCNP development is supported by the US Department of Energy's National Security Administration – Advanced Simulation and Computing (NNSA-ASC).

## References

- 1) T. Goorley, M. James, T. Booth, F. Brown, J. Bull, L.J. Cox, J. Durkee, J. Elson, M. Fensin, R.A. Forster, J. Hendricks, H.G. Hughes, R. Johns, B. Kiedrowski, R. Martz, S. Mashnik, G. McKinney, D. Pelowitz, R. Prael, J. Sweezy, L. Waters, T. Wilcox, T. Zukaitis, Initial MCNP6 Release Overview, LA-UR-11-01766, *Nuclear Technology* 180 (298-315) December 2012.
- 2) X-5 Monte Carlo Team, *MCNP — A General Monte Carlo N-Particle Transport Code, Version 5 — Volume I: Overview and Theory*, LA-UR-03-1987, revised 2/2008 (2008).
- 3) D. Pelowitz (ed.), *MCNPX User's Manual, Version 2.7.0*, LA-CP-11-00438 (2011).

- 4) Members of the Cross Section Evaluation Working Group, ENDF-6 Formats Manual, CSEWG Document ENDF-102, BNL-90365-2009, (2009).
- 5) S. M. Seltzer, "An Overview of ETRAN Monte Carlo Methods," in *Monte Carlo Transport of Electrons and Photons*, ed. T. M. Jenkins, W. R. Nelson and A. Rindi, Plenum Press, New York (1988) ISBN 0-306-43099-1.
- 6) J. S. Hendricks and A. C. Kahler, "MCNP/X Form Factor upgrade for Improved Photon Transport," *Proceedings of the RPSD2010*, April 18-23, 2010, Las Vegas, Nevada, LA-UR-10-00213 (2010).
- 7) C. Toccoli, private communication.
- 8) G. Molière, Theorie der Streuung schneller geladener Teilchen I: Einzelstreuung am abgeschirmten Coulomb-Feld, *Z. Naturforsch.* 2a (1947) 133.
- 9) D. E. Cullen, M. H. Chen, J. H. Hubbell, S. T. Perkins, E. F. Plechaty, J. A. Rathkopf and J. H. Scofield, *Tables and Graphs of Photon-Interaction Cross Sections from 10 eV to 100 GeV*, UCRL50400, V. 6, Parts A and B (1989).